Macromolecules

pubs.acs.org/Macromolecules Article

Dynamics of Flexible Viruses in Polymer Solutions

Maxwell Smith, Ryan Poling-Skutvik, Ali H. Slim, Richard C. Willson,* and Jacinta C. Conrad*

Cite This: *Macromolecules* 2021, 54, 4557−4563 Read Online

ACCESS | Metrics & More | Article Recommendations | Supporting Information

ABSTRACT: We examine the coupling of the dynamics of flexible viral nanoparticles to the dynamics of comparably sized polymer chains. Using fluorescence microscopy, we quantify the dynamics of three filamentous viruses, potato virus M (PVM), M13, and pf1, that are suspended in semidilute solutions of partially hydrolyzed polyacrylamide. The dynamics of the viral nanoparticles are approximately diffusive on accessible time and length scales, but the distributions of displacements are non-Gaussian and exhibit increasingly extended tails as the aspect ratio of the viruses or the polymer concentration is increased. The long-time diffusion coefficients do not collapse onto a universal curve based on existing models for rodlike or spherical nanoparticles that are comparably sized to the polymer chains. Instead, the diffusivities appear to collapse as a function of the ratio of the polymer correlation length and a length scale intermediate between the virus radius and length, indicating that the hydrodynamic coupling to the polymer dynamics is affected by the virus anisotropy and flexibility.

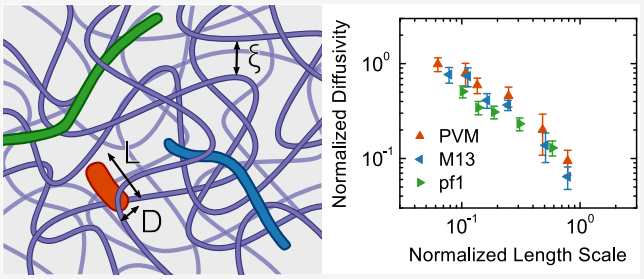

INTRODUCTION

Highly anisotropic nanoparticles are used to impart desired functionality to polymer nanocomposites,[1,2] to deliver drugs and therapeutic agents in nanomedicine,[3] and as nanoscale viscometers in complex fluids.[4] The transport of anisotropic particles in polymer solutions and melts, essential for these applications, is expected to differ from that of micron-sized spherical particles. For spherical nanoparticles, the Stokes−Einstein (SE) equation $D_{SE} = k_B T/6\pi\eta R_{NP}$ relates the diffusion coefficient D_{SE} of a particle of radius R to the viscosity η of the background fluid, which is assumed to be homogeneous. The assumption that a complex fluid is homogeneous is not valid, however, when the length scales of the particle and the fluid are comparable, as is often found for nanoparticles in polymer media. Thus, the diffusivity of nanoparticles in polymer solutions and melts can strongly deviate from the SE prediction.[5−9] Several theories and models have been developed to describe nanoparticle dynamics in polymeric matrices. In obstruction models, polymer coils are treated as static and rigid objects around which the particle must move.[10−12] Hydrodynamic models, alternatively, posit that polymers interact with particles through viscous drag and predict that hydrodynamic interactions are screened over the polymer correlation length ξ.[6,13,14] Scaling models extend hydrodynamic theories to account for the coupling between the particle dynamics and those of the surrounding polymer chains.[15−17]

These theories, however, were developed for isotropic, spherical nanoparticles and may not be readily applicable to anisotropic particles, which are characterized by multiple length scales.[4,18] Even in Newtonian fluids, nanorods experience different viscous forces and angular moments than nanospheres of an equal radius.[19−22] In polymer systems, nanorods with aspect ratios AR = L/R of order 10 violate Stokes−Einstein predictions to diffuse faster than spherical particles of a similar hydrodynamic radius when the nanorod diameter $2R$ is comparable to characteristic polymer length scales.[23−26] Further, as AR increases, the nanorod translational diffusivity D_t decreases more slowly than rotational diffusivity D_r.[26,27] Tuning the interactions between the nanorod and the polymer matrix can also increase the diffusivity of nanorods.[28] While these comparisons have provided important insights into how to tune diffusion, how anisotropic particles experience local structural heterogeneities remains incompletely understood. Intriguingly, the fact that the enhanced diffusivity of nanorods diminishes as L/R is increased[26,28] suggests that a competition between L and R controls nanorod diffusion.

Here, we measure the dynamics of semiflexible, anisotropic virus particles as model nanorods with large aspect ratios in semidilute polymer solutions. Using fluorescence microscopy, we quantify the dynamics of three labeled filamentous viruses, PVM, M13, and pf1, in solutions of partially hydrolyzed polyacrylamide. The long-time diffusion coefficients of the filamentous viral nanoparticles are an order of magnitude faster than expected but do not collapse onto a universal curve based

Received: February 23, 2021
Revised: April 19, 2021
Published: May 4, 2021

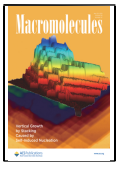

https://doi.org/10.1021/acs.macromol.1c00435
Macromolecules 2021, 54, 4557−4563

on existing models for rods[19−21,29] or spheres.[16] Instead, the long-time diffusion coefficients can be collapsed onto a master curve as a function of the ratio of the polymer correlation length ξ and a length scale between virus L and R. This collapse demonstrates the important role of particle length scales on the dynamics of highly anisotropic viral nanoparticles in polymer solutions.

MATERIALS AND METHODS

Viral and Spherical Particles. Three different filamentous viral nanoparticles were used in these experiments: a plant virus, potato virus M (PVM; ASLA biotech), and two filamentous bacteriophages (viruses that infect bacteria), M13 (Guild Biosciences) and pf1 (ASLA biotech) (Figure 1a).[30] M13[31] and pf1[32] are semiflexible

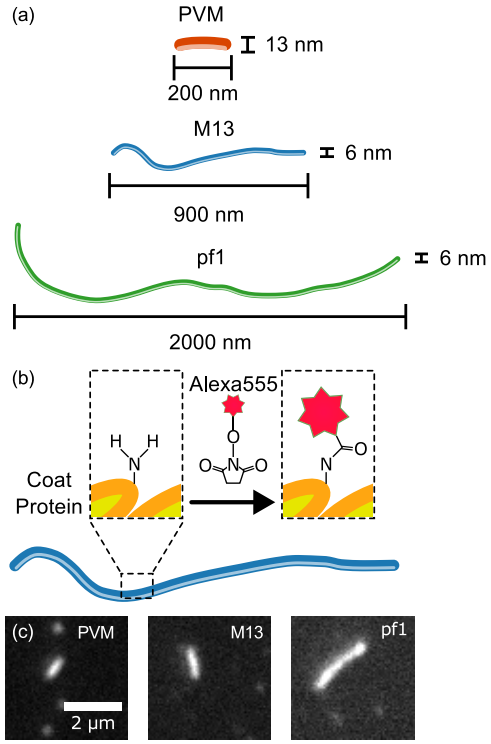

Figure 1. Virus preparation. (a) Schematics of PVM (orange), M13 (blue), and pf1 (green) viruses. (b) Schematic of fluorescence labeling of the virus major coat protein with Alexa555 using NHS and primary amine chemistry. (c) Fluorescence micrographs of fluorescently labeled virus particles on the surface of an unmodified glass slide.

viruses whose persistence length $L_p \cong 2$ μm is comparable to their contour length L = 900 nm and 2 μm, respectively. Although the persistence length for PVM has not been reported, the viral coat protein assembly of PVM[33] is similar to that of M13 and pf1. Therefore, we hypothesize that the L_p of PVM is comparable to that of M13 and pf1. The ratio $L_p/L \cong 0.1$ for PVM (L = 200 nm) suggests that PVM behaves as a rigid rod. Three spherical fluorescent polystyrene particles of diameters 100 nm, 300 nm, and 2 μm (Fluoro-Max Red Aqueous Fluorescent Particles, excitation and emission wavelengths of 542 and 612 nm, respectively; Thermo Fisher Scientific) were used as control particles.

Poly(ethylene glycol) (PEG) Precipitation of PVM. To increase the PVM concentration in the stock solutions prior to functionalization, PVM particles were precipitated using a 20% w/v solution of poly(ethylene glycol) (PEG, weight average molecular weight 7450× g mol^{-1}; Spectrum Chemical Manufacturing Corp.) in 2.5 M sodium chloride solution at a volume ratio of 1 part PEG solution to 5 parts stock PVM solution. The PVM/polymer solution was incubated with PEG for 1 h at 4 °C and then centrifuged for 30 min at 3200g, after which the virus particles were resuspended in 1X PBS (1X phosphate-buffered saline solution). Because stock concentrations of M13 and pf1 were sufficiently high, these samples did not require concentration prior to functionalization.

Functionalization of Virus Particles. Viruses were labeled with the fluorescent dye Alexa555 (Alexa Fluor 555 NHS Ester, excitation and emission wavelengths of 488 and 532 nm, respectively; Thermo Fisher Scientific). The *N*-hydroxysuccinimide (NHS) group covalently bonds to the primary amines of the coat protein's N-terminus (Figure 1b).[34] The virus stock (100 μL) was buffer-exchanged from the storage buffer to the dye conjugation buffer, 0.2 M sodium bicarbonate at pH 8.3, using a Zeba column (Zeba Spin Desalting Column, 7K MWCO; Thermo Fisher Scientific). After buffer exchange, 10 μL of Alexa555 dye solution (10 mg mL^{-1} Alexa555 in dimethyl sulfoxide; Thermo Fisher Scientific) was added to the buffer-exchanged virus solution and incubated overnight at 4 °C. The virus-dye solutions were dialyzed with a Float-A-Lyzer (Float-A-Lyzer Dialysis Device; Spectrum Laboratories Inc.) to remove any unreacted dye. Solutions containing M13 and pf1 were dialyzed with a 1 mL, 100 kD MWCO Float-A-Lyzer. Solutions containing PVM, the smallest virus, were first PEG precipitated, resuspended in 1X PBS, and then dialyzed using a 1 mL, 3.5−5 kD MWCO Float-A-Lyzer. The dialysis buffer volume (1 L) was changed after 2 h for three cycles at room temperature and then overnight at room temperature. After dialysis, dyed virus particles were imaged using fluorescence microscopy to confirm the success of the dyeing protocol.

Preparation of Virus−Polymer Solutions. Partially hydrolyzed polyacrylamide (HPAM, FLOPAAM 3330; SNF) was used as a model crowding agent. To determine the overlap concentration, the viscosity as a function of HPAM concentration in 1X PBS was measured using an Ubbelohde viscometer (Supporting Information). The intrinsic viscosity $[\eta]$ = 3.2 L g^{-1} was extracted from the first-order pseudovirial expansion of viscosity η as a function of polymer mass concentration c, $\eta = \eta_0 (1 + [\eta]\, c)$. The overlap concentration c^* = 0.31 g L^{-1} was estimated as the inverse of the intrinsic viscosity $c^* = 1/[\eta]$. The radius of gyration R_g = 220 nm of the HPAM in 1X PBS was then calculated using

$$R_{g,0} = \left(\frac{M_w}{\frac{4}{3}\pi N_{av}[\eta]} \right)^{1/3} \quad (1)$$

where $M_w = 8 \times 10^6$ g mol^{-1} is the molecular weight of HPAM and N_{av} is Avogadro's number. Homogeneous HPAM/PBS stock solutions were prepared by mixing HPAM in 1× PBS at a concentration of 18.6 mg mL^{-1} using a tube roller for 1 week at room temperature to create a 60c^* stock solution. Polymer solutions were prepared by diluting the homogenized stock solution to the desired concentration. Virus particles were added to the homogenized polymer solutions and allowed to equilibrate overnight at 4 °C.

Imaging and Tracking of Viruses. Viral nanoparticles were imaged in air-tight sample chambers consisting of glass microscope slides (Gold Seal Cover Glass; Thermo Fisher Scientific) that were sealed with Norland Optical Adhesive 81 (Norland Products). To reduce the nonspecific binding of viruses on the surface of the sample chambers, microscope slides were coated with BSA (bovine serum albumin heat shock fraction, pH 7, ≥98 %; Thermo Fisher Scientific) prior to chamber assembly. Slides were soaked in a solution of 2.5% w/v BSA in water for 1 h at room temperature. After soaking, the slides were wiped carefully with Kimwipes to remove excess liquid and dried, covered, overnight at room temperature.

Viral nanoparticles suspended in polymer solutions were imaged on a DMI3000 B microscope (Leica) furnished with an HCX PL APO 100×/1.40−0.70 oil immersion objective (Leica) and an N2.1 filter cube (Leica) using an sCMOS pco.edge 4.2 m camera (PCOTM) at 20 frames per second and 50 ms exposure time. The focus of the objective lens was positioned at least 20 μm away from the bottom surface of the sample chamber to minimize any effects from the

https://doi.org/10.1021/acs.macromol.1c00435
Macromolecules 2021, 54, 4557−4563

chamber surfaces. Five microscope videos with 1000 frames per video were captured and analyzed using particle-tracking algorithms[35] to obtain particle trajectories. Although the virus dimensions cannot be directly extracted from microscopy because the virus nanoparticle diameter is below the optical diffraction limit, the centroids of the viruses can still be imaged and tracked over time.

From the particle trajectories, the one-dimensional, ensemble-averaged mean-squared displacement (MSD) $\langle \Delta x^2 \rangle$ was calculated as a function of lag time Δt. For each polymer solution concentration, D_t was extracted from a linear fit of the long-time MSD versus lag time via $\langle \Delta x^2(\Delta t) \rangle = 2D_t \Delta t$. We also calculated the probability distribution of displacements (PDD) $G_s(\Delta x, \Delta t) = \frac{1}{N} \langle \sum_{i=1}^{N} \delta(x_i(t) - x_i(t + \Delta t) - \Delta x) \rangle$,[35] which measures the probability of a particle displacing a distance Δx at a lag time Δt.

RESULTS AND DISCUSSION

Viral Nanoparticle Dynamics. We first examine the diffusivity of viral nanoparticles in the absence of the polymer. The MSDs of PVM (aspect ratio AR of 15), M13 (AR of 150), and pf1 (AR of 330) suspended in 1X PBS scale approximately linearly with Δt. From a linear fit of the MSDs, we determine the translational diffusivities D_0 as 1.63 ± 0.07, 1.57 ± 0.12, and 2.02 ± 0.14 $\mu m^2\ s^{-1}$ for PVM, M13, and pf1, respectively. The corresponding hydrodynamic radii, determined using the SE equation, are 131 ± 6, 136 ± 11, and 106 ± 8 nm for PVM, M13, and pf1, respectively. The diffusivity measured for M13 in dilute solution is in reasonable agreement with earlier measurements of the diffusivity of another Ff bacteriophage, the closely related and structurally similar *fd* virus,[36,37] and is somewhat larger than the diffusivity of M13 in concentrated solutions near the isotropic-to-nematic transition.[38] The hydrodynamic radii of M13 and pf1 are much smaller than the radius of gyration of rigid rods of corresponding length and width (520 and 1200 nm, respectively, for M13 and pf1), suggesting that these viruses behave as semiflexible particles. This observation is consistent with expectations based on the ratio of virus persistence length L_p and contour length L, which for M13 and pf1 are 0.45 and 1.0, respectively.[31,32] The measured hydrodynamic radius of PVM, however, is close to that of its rigid-rod counterpart (120 nm), consistent with $L_p/L = 0.1$.

The MSDs of PVM, M13, and pf1 scale approximately linearly with Δt for all c/c^* within the experimental error. This linearity indicates that the viral nanoparticles move diffusively through the polymer solution on all accessible time scales (Figure 2). Similar diffusive behavior has been observed for other anisotropic nanoparticles, including colloidal nanorods diffusing through polymeric[28] and mucosal gels,[39] entangled wormlike micelle solutions,[40] and semidilute and entangled polymer solutions.[24] Likewise, the MSDs of spherical particles scale linearly with Δt on accessible time scales (Supporting Information). Additionally, the virus MSDs decrease with increasing c/c^* as the viscosity of the polymer solutions increases. The MSDs represent an ensemble average of the particle dynamics but do not provide information on how individual particles move through the solutions. Thus, to elucidate the microscopic processes that control viral nanoparticle transport, we next examine the distributions of particle displacements.

Even though the virus MSDs increase linearly with time, the PDDs $G_s(\Delta x, \Delta t)$ are strongly non-Gaussian for all three viral nanoparticles (PVM, M13, pf1) and for all polymer concentrations (Figure 3). To compare the dynamics of

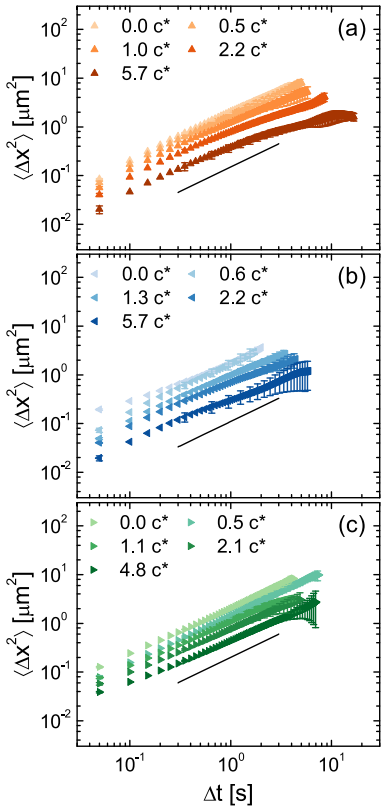

Figure 2. Mean-squared displacement $\langle \Delta x^2 \rangle$ as a function of lag time Δt for viral nanoparticles (a) PVM, (b) M13, and (c) pf1 at various polymer concentrations. Solid reference lines represent linear scaling.

particles at different c/c^*, we normalize the displacement Δx by the diffusive displacement at a lag time Δt $(2D_t \Delta t)^{1/2}$. For a given virus, the extended tails of the PDDs more strongly deviate from the Gaussian prediction as c/c^* is increased. Both the maximum displacement and the probability of large displacements increase with the polymer concentration. Similarly, for a constant c/c^*, the non-Gaussianity of the PDDs is enhanced as the virus AR is increased (PVM < M13 < pf1). These two effects result in smaller deviations from the Gaussian distribution for PVM and larger deviations for pf1 (Figure 4). Thus, these viral nanoparticles exhibit Fickian but non-Gaussian dynamics[41] in semidilute polymer solutions. These dynamics may arise from one or more mechanisms. The displacement distributions include contributions from motions both parallel to and perpendicular to the long axis of the phage. The relative contributions likely change as the phage aspect ratio is increased and as the medium response becomes increasingly non-Newtonian (i.e., as the polymer concentration is increased). Additionally, non-Gaussian PDDs are reported for shapes in which the center of hydrodynamic stress does not coincide with the center of tracking.[42,43] This effect may also contribute to the pronounced non-Gaussian PDDs of the semiflexible M13 and pf1.

Fickian diffusion concurrent with non-Gaussian displacement distributions has been widely reported for particles in complex fluids.[44−48] This behavior is often attributed to a distribution of diffusivities,[41,44,49] which can arise as particles experience distinct local environments due to structural heterogeneities; through spatial and temporal variations in hydrodynamic interactions through the medium; or through the formation and breaking of transient cages, leading to

https://doi.org/10.1021/acs.macromol.1c00435
Macromolecules 2021, 54, 4557−4563

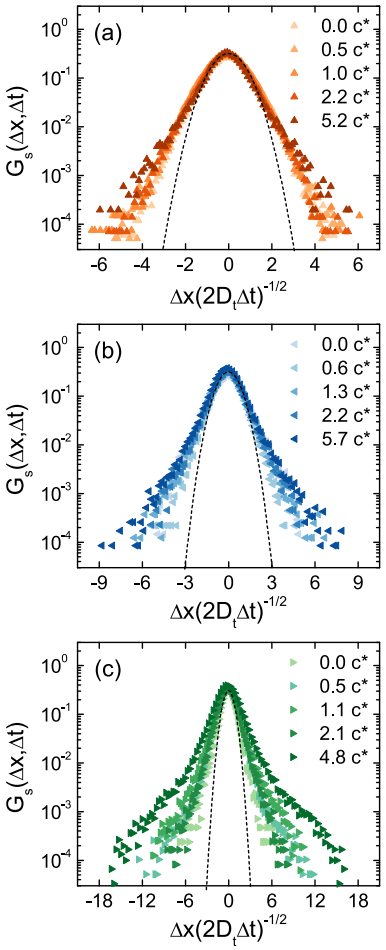

Figure 3. Normalized probability distribution of displacements $G_s(\Delta x, \Delta t)$ as a function of normalized displacement $\Delta x(2D_t\Delta t)^{-1/2}$ for virus particles (a) PVM, (b) M13, and (c) pf1 at Δt = 0.05 s in solutions of various polymer concentrations c/c^*. The dashed line indicates a Gaussian distribution.

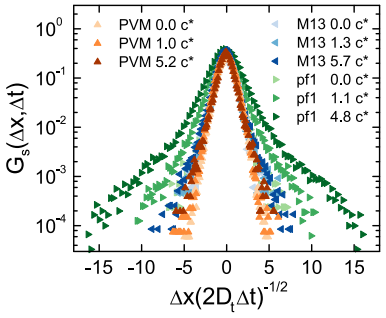

Figure 4. Comparison of virus normalized probability distributions of displacements $G_s(\Delta x, \Delta t)$ as a function of normalized displacement $\Delta x(2D_t\Delta t)^{-1/2}$ for virus particles PVM (orange upright triangles), M13 (blue left-pointing triangles), and pf1 (green right-pointing triangles) at polymer concentrations c/c^* below and above the overlap concentration.

activated hopping.[16,17,40,50−52] To assess the importance of structural heterogeneities for non-Gaussian dynamics, we calculated the PDDs for spherical particles of comparable hydrodynamic radii in the polymer solutions. The PDDs collapse onto a single Gaussian distribution for all spherical particles and for all c/c^* (Supporting Information). This result is consistent with earlier studies of spherical particles in semidilute polymer solutions[48,53,54] and suggests that structural heterogeneities in the solution do not control the non-Gaussian dynamics exhibited by the viruses. The solutions are formulated at concentrations below the entanglement concentration of HPAM in 1X PBS (c_E > 20c^*, Supporting Information), indicating that entanglements do not contribute to the non-Gaussian dynamics. Similarly, neither reptation[55−57] nor hopping mechanisms can explain viral nanoparticle dynamics in solutions of concentration less than c_E.

Instead, we hypothesize that the anisotropy of filamentous viruses gives rise to the non-Gaussian distributions observed for virus dynamics. Filamentous viruses are characterized by two length scales, their radius R and width L. We posit that the two characteristic length scales result in different degrees of coupling between viral nanoparticle dynamics and those of the polymer in solution when the virus displaces parallel or perpendicular to its major axis. Differences in the hydrodynamic drag forces acting on each of these modes then lead to a distribution of diffusivities. In support of this picture, we note that the extended tails of the non-Gaussian distributions become more prominent as the AR of the virus increases (Figure 4), which we expect exaggerates the difference in hydrodynamics between parallel and perpendicular modes. These differences in coupling are also likely to affect the dependence of the ensemble-averaged diffusivities on the polymer concentration.

Scaling of the Long-Time Diffusivity. To determine the effects of the multiple diffusive modes on the transport of viral nanoparticles, we compare the long-time translational diffusivities of the viruses (extracted from the ensemble-averaged MSDs in Figure 2) to those of spherical nanoparticles. The normalized diffusivities of spherical particles, for which the PDDs are Gaussian, collapse onto a single curve as a function of c/c^* (Figure 5). This result indicates that the

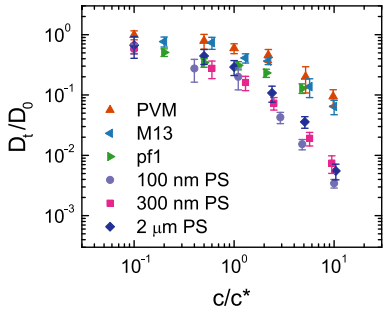

Figure 5. Normalized diffusivity D_t/D_0 as a function of normalized polymer concentration c/c^*.

dynamics of spherical nanoparticles follow the SE prediction obtained using the bulk viscosity. In sharp contrast, the virus diffusivities do not collapse on this SE master curve. Instead, the virus diffusivities are up to 30 times greater than the SE prediction.

Faster-than-expected dynamics in polymer solutions have been observed for spherical nanoparticles whose size is comparable to length scales characterizing the polymer (R_g, ξ).[24,53,54] In this size regime, the dynamics of the particles decouple from the solution viscosity and instead couple to the dynamics of the polymer chains.[16] This coupling is controlled by the particle size, resulting in dynamics that collapse as a function of R/ξ. For anisotropic nanoparticles, however, it is

https://doi.org/10.1021/acs.macromol.1c00435
Macromolecules 2021, 54, 4557−4563

not clear which length scale or scales control the particle diffusivity. The non-Gaussianity of the PDDs suggests that both the radius and length play a role in how filamentous viruses move through polymer solutions. We therefore examine the dependence of the diffusivity on R, L, and their combinations (Table 1).

Table 1. Different Length Scales S_i for PVM, M13, and pf1 Virus Particles

S_i [nm]	L	$2R$	$\frac{L}{\ln(L/R)}$	$\frac{R}{\ln(L/R)}$	R_V	R_{SA}
PVM	200	13	58	3.8	29	25
M13	900	6	160	1.0	29	37
pf1	2000	6	310	0.9	38	55

We first examine the dependence of the normalized translational diffusivity D_t/D_0 on L/ξ and R/ξ (Figure 6a,b). Neither ratio is able to collapse the virus diffusivities onto a single curve. Whereas L/ξ shifts the diffusivities of the high-AR (pf1) virus to larger length scales relative to those of the short-AR PVM, R/ξ conversely shifts PVM to larger effective length scales. We conclude that the controlling length scale must be intermediate between R and L.

In Newtonian liquids, the dynamics of rigid rods are dissimilar in directions parallel and perpendicular to the major axis due to differences in the hydrodynamic drag equations. The hydrodynamic modes average to produce a length scale of $L/\ln(L/R)$[21] that controls the frictional drag and hence the translational diffusivity. Neither this length scale nor its radial counterpart $R/\ln(L/R)$, however, is able to collapse the diffusivity data for the viral nanoparticles onto a single curve (Figure 6c,d). This result indicates that the ratio of the hydrodynamic drag forces acting in the directions parallel and perpendicular to the virus major axis is different in polymer solutions than in Newtonian simple fluids. Further, it also indicates that the hydrodynamic radius of filamentous viruses, measured in 1X PBS (a Newtonian fluid), cannot be used to predict virus dynamics in semidilute polymer solutions.

Finally, a standard approach to determine the hydrodynamic forces on an anisotropic particle is to evaluate the frictional coefficients using a spherical particle of equivalent size as the basis for the Reynolds number Re_{eq}.[58−61] Inspired by this approach, we attempt to map the anisotropy of the viral nanoparticles onto spheres of an equivalent size through two effective length scales $R_V = (3R^2L/4)^{1/3}$ and $R_{SA} = (RL/2)^{1/2}$ (Table 1). These length scales represent a sphere of equivalent volume or surface area to the virus. Both length scales collapse the normalized virus diffusivities onto a single curve within experimental error (Figure 6e,f). Given the error in our measurements, we cannot conclude which of these length scales controls virus diffusion in semidilute polymer solutions. Nonetheless, both collapses support the idea that virus diffusivity depends on a weighted average of the radius and the length of the viral nanoparticle. This finding is consistent with the observation of non-Gaussian PDDs (Figure 3) and with the hypothesis that virus anisotropy leads to differences in the hydrodynamic drag forces that act on motions parallel and perpendicular to the long axis.

CONCLUSIONS

We measured the dynamics of three filamentous viruses in semidilute solutions of the polymer using optical microscopy. Although the dynamics of the viral nanoparticles are diffusive on accessible time scales, the distributions of particle displacements are strikingly non-Gaussian and feature extended tails that become more pronounced as either the polymer concentration or virus aspect ratio is increased. We attribute the non-Gaussian displacement distributions to the presence of multiple diffusive modes as filamentous viruses move along and normal to their major axis. These diffusive modes are different than those predicted by spherical or rigid-rod scaling theories. Through these multiple diffusive modes, filamentous viruses are able to diffuse through semidilute polymer solutions over an order of magnitude faster than spherical nanoparticles of comparable size. The faster-than-expected diffusivities can be collapsed onto single curves according to effective length scales that are intermediate

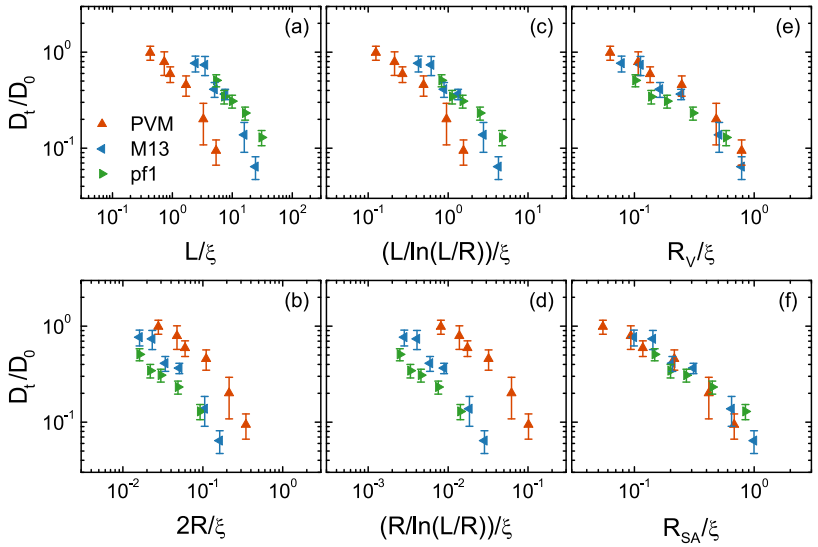

Figure 6. Normalized diffusivity D_t/D_0 of the different virus species as a function of normalized length scale S_i/ξ, where S_i is the (a) virus length L, (b) virus diameter $2R$, (c) virus length, and (d) virus radius scaled by the natural log of virus length over radius $L/\ln(L/R)$ and $R/\ln(L/R)$ and virus radius of a sphere of equivalent (e) volume R_V and (f) surface area R_{SA}, where ξ is the polymer correlation length.

https://doi.org/10.1021/acs.macromol.1c00435
Macromolecules 2021, 54, 4557−4563

between R and L, consistent with the idea that filamentous viruses move through parallel and perpendicular motions.

Viruses are useful as tunable model systems for anisotropic particle transport in complex media, as their persistence length[62,63] and contour length[64] can be modified by controlled mutation. Importantly, the filamentous viruses examined here, like λ-phage,[65,66] are semiflexible. Earlier studies on semiflexible carbon nanotubes showed that flexibility controlled their diffusion through polymer gels.[56] We speculate that the differences in the diffusive modes of filamentous viruses are related to the flexibility of the viral nanoparticles and the corresponding segmental dynamics[56,57,65,66] and plan to explore the role of flexibility in future work.

■ ASSOCIATED CONTENT

Supporting Information

The Supporting Information is available free of charge at https://pubs.acs.org/doi/10.1021/acs.macromol.1c00435.

Rheology of HPAM in 1X PBS, Zimm and Rouse relaxation times of HPAM, virus particle diffusive times, mean-squared displacements and probability distribution of displacements of spherical particles, DLS measurements of spherical particles in dilute HPAM solutions (PDF)

■ AUTHOR INFORMATION

Corresponding Authors

Richard C. Willson − *Department of Chemical and Biomolecular Engineering, University of Houston, Houston, Texas 77204-4004, United States;* orcid.org/0000-0002-0900-6148; Email: willson@uh.edu

Jacinta C. Conrad − *Department of Chemical and Biomolecular Engineering, University of Houston, Houston, Texas 77204-4004, United States;* orcid.org/0000-0001-6084-4772; Email: jcconrad@uh.edu

Authors

Maxwell Smith − *Department of Chemical and Biomolecular Engineering, University of Houston, Houston, Texas 77204-4004, United States*

Ryan Poling-Skutvik − *Department of Chemical Engineering, University of Rhode Island, Kingston, Rhode Island 02881, United States;* orcid.org/0000-0002-1614-1647

Ali H. Slim − *Department of Chemical and Biomolecular Engineering, University of Houston, Houston, Texas 77204-4004, United States*

Complete contact information is available at: https://pubs.acs.org/10.1021/acs.macromol.1c00435

Notes

The authors declare no competing financial interest.

■ ACKNOWLEDGMENTS

The authors gratefully acknowledge funding from the Welch Foundation (E-1869) and NSF (CBET-1803728).

■ REFERENCES

(1) Mitchell, C. A.; Bahr, J. L.; Arepalli, S.; Tour, J. M.; Krishnamoorti, R. Dispersion of functionalized carbon nanotubes in polystyrene. *Macromolecules* **2002**, *35*, 8825−8830.

(2) Ferrier, R. C.; Lee, H.-S.; Hore, M. J. A.; Caporizzo, M.; Eckmann, D. M.; Composto, R. J. Gold nanorod linking to control plasmonic properties in solution and polymer nanocomposites. *Langmuir* **2014**, *30*, 1906−1914.

(3) Meyer, R. A.; Green, J. J. Shaping the future of nanomedicine: anisotropy in polymeric nanoparticle design. *Wiley Interdiscip. Rev. Nanomed. Nanobiotechnol.* **2016**, *8*, 191−207.

(4) Molaei, M.; Atefi, E.; Crocker, J. C. Nanoscale rheology and anisotropic diffusion using single gold nanorod probes. *Phys. Rev. Lett.* **2018**, *120*, 118002.

(5) Ye, X.; Tong, P.; Fetters, L. J. Transport of probe particles in semidilute polymer solutions. *Macromolecules* **1998**, *31*, 5785−5793.

(6) Cheng, Y.; Prud'homme, R. K.; Thomas, J. L. Diffusion of mesoscopic probes in aqueous polymer solutions measured by fluorescence recovery after photobleaching. *Macromolecules* **2002**, *35*, 8111−8121.

(7) Mackay, M. E.; Dao, T. T.; Tuteja, A.; Ho, D. L.; Van Horn, B.; Kim, H.-C.; Hawker, C. J. Nanoscale effects leading to non-Einstein-like decrease in viscosity. *Nat. Mater.* **2003**, *2*, 762−766.

(8) Tuteja, A.; Mackay, M. E.; Narayanan, S.; Asokan, S.; Wong, M. S. Breakdown of the continuum Stokes-Einstein relation for nanoparticle diffusion. *Nano Lett.* **2007**, *7*, 1276−1281.

(9) Pryamitsyn, V.; Ganesan, V. Noncontinuum effects on the mobility of nanoparticles in unentangled polymer solutions. *J. Polym. Sci., Part B: Polym. Phys.* **2016**, *54*, 2145−2150.

(10) Ogston, A. G. The spaces in a uniform random suspension of fibres. *Trans. Faraday Soc.* **1958**, *54*, 1754−1757.

(11) Altenberger, A. R.; Tirrell, M. On the theory of self-diffusion in a polymer gel. *J. Chem. Phys.* **1984**, *80*, 2208−2213.

(12) Johansson, L.; Elvingson, C.; Löfroth, J.-E. Diffusion and interaction in gels and solutions. 3. Theoretical results on the obstruction effect. *Macromolecules* **1991**, *24*, 6024−6029.

(13) Cukier, R. I. Diffusion of Brownian spheres in semidilute polymer solutions. *Macromolecules* **1984**, *17*, 252−255.

(14) Phillies, G. D. J.; Ullmann, G. S.; Ullmann, K.; Lin, T. H. Phenomenological scaling laws for "semidilute" macromolecule solutions from light scattering by optical probe particles. *J. Chem. Phys.* **1985**, *82*, 5242−5246.

(15) Brochard Wyart, F.; de Gennes, P. G. Viscosity at small scales in polymer melts. *Eur. Phys. J. E: Soft Matter Biol. Phys.* **2000**, *1*, 93−97.

(16) Cai, L.-H.; Panyukov, S.; Rubinstein, M. Mobility of nonsticky nanoparticles in polymer liquids. *Macromolecules* **2011**, *44*, 7853−7863.

(17) Cai, L.-H.; Panyukov, S.; Rubinstein, M. Hopping diffusion of nanoparticles in polymer matrices. *Macromolecules* **2015**, *48*, 847−862.

(18) Tsay, J. M.; Doose, S.; Weiss, S. Rotational and translational diffusion of peptide-coated CdSe/CdS/ZnS nanorods studied by fluorescence correlation spectroscopy. *J. Am. Chem. Soc.* **2006**, *128*, 1639−1647.

(19) Broersma, S. Viscous Force Constant for a Closed Cylinder. *J. Chem. Phys.* **1960**, *32*, 1632−1635.

(20) Broersma, S. Rotational diffusion constant of a cylindrical particle. *J. Chem. Phys.* **1960**, *32*, 1626−1631.

(21) Tirado, M. M.; de la Torre, J. G. Rotational dynamics of rigid, symmetric top macromolecules. Application to circular cylinders. *J. Chem. Phys.* **1980**, *73*, 1986−1993.

(22) Vasanthi, R.; Bhattacharyya, S.; Bagchi, B. Anisotropic diffusion of spheroids in liquids: Slow orientational relaxation of the oblates. *J. Chem. Phys.* **2002**, *116*, 1092−1096.

(23) Lee, K. L.; Hubbard, L. C.; Hern, S.; Yildiz, I.; Gratzl, M.; Steinmetz, N. F. Shape matters: the diffusion rates of TMV rods and CPMV icosahedrons in a spheroid model of extracellular matrix are distinct. *Biomater. Sci.* **2013**, *1*, 581−588.

(24) Alam, S.; Mukhopadhyay, A. Translational and rotational diffusions of nanorods within semidilute and entangled polymer solutions. *Macromolecules* **2014**, *47*, 6919−6924.

(25) Choi, J.; Cargnello, M.; Murray, C. B.; Clarke, N.; Winey, K. I.; Composto, R. J. Fast nanorod diffusion through entangled polymer melts. *ACS Macro Lett.* **2015**, *4*, 952−956.

(26) Karatrantos, A.; Composto, R. J.; Winey, K. I.; Clarke, N. Nanorod diffusion in polymer nanocomposites by molecular dynamics simulations. *Macromolecules* **2019**, *52*, 2513−2520.
(27) Kim, J.; Adhikari, M.; Dhamane, S.; Hagström, A. E. V.; Kourentzi, K.; Strych, U.; Willson, R. C.; Conrad, J. C. Detection of viruses by counting single fluorescent genetically biotinylated reporter immunophage using a lateral flow assay. *ACS Appl. Mater. Interfaces* **2015**, *7*, 2891−2898.
(28) Wang, J.; Yang, Y.; Yu, M.; Hu, G.; Gan, Y.; Gao, H.; Shi, X. Diffusion of rod-like nanoparticles in non-adhesive and adhesive porous polymeric gels. *J. Mech. Phys. Solids* **2018**, *112*, 431−457.
(29) de la Torre, J. G.; Martinez, M. C. L.; Tirado, M. M. Dimensions of short, rodlike macromolecules from translational and rotational diffusion coefficients. Study of the gramicidin dimer. *Biopolymers* **1984**, *23*, 611−615.
(30) Kim, J.; Vu, B.; Kourentzi, K.; Willson, R. C.; Conrad, J. C. Increasing binding efficiency via reporter shape and flux in a viral nanoparticle lateral-flow assay. *ACS Appl. Mater. Interfaces* **2017**, *9*, 6878−6884.
(31) Barry, E.; Beller, D.; Dogic, Z. A model liquid crystalline system based on rodlike viruses with variable chirality and persistence length. *Soft Matter* **2009**, *5*, 2563−2570.
(32) Dogic, Z.; Fraden, S. Smectic phase in a colloidal suspension of semiflexible virus particles. *Phys. Rev. Lett.* **1997**, *78*, 2417−2420.
(33) Kalnciema, I.; Balke, I.; Skrastina, D.; Ose, V.; Zeltins, A. Potato Virus M-like nanoparticles: Construction and characterization. *Mol. Biotechnol.* **2015**, *57*, 982−992.
(34) Kim, J.; Poling-Skutvik, R.; Trabuco, J. R. C.; Kourentzi, K.; Willson, R. C.; Conrad, J. C. Orientational binding modes of reporters in a viral-nanoparticle lateral flow assay. *Analyst* **2017**, *142*, 55−64.
(35) Crocker, J. C.; Grier, D. G. Methods of digital video microscopy for colloidal studies. *J. Colloid Interface Sci.* **1996**, *179*, 298−310.
(36) Newman, J.; Swinney, H. L.; Day, L. A. Hydrodynamic properties and structure of fd virus. *J. Mol. Biol.* **1977**, *116*, 593−603.
(37) Maeda, T.; Fujime, S. Dynamic light-scattering study of suspensions of fd virus. Application of a theory of light-scattering spectrum of weakly bending filaments. *Macromolecules* **1985**, *18*, 2430−2437.
(38) Lettinga, M. P.; Barry, E.; Dogic, Z. Self-diffusion of rod-like viruses in the nematic phase. *Europhys. Lett.* **2005**, *71*, 692−698.
(39) Yu, M.; Wang, J.; Yang, Y.; Zhu, C.; Su, Q.; Guo, S.; Sun, J.; Gan, Y.; Shi, X.; Gao, H. Rotation-facilitated rapid transport of nanorods in mucosal tissues. *Nano Lett.* **2016**, *16*, 7176−7182.
(40) Lee, J.; Grein-Iankovski, A.; Narayanan, S.; Leheny, R. L. Nanorod mobility within entangled wormlike micelle solutions. *Macromolecules* **2017**, *50*, 406−415.
(41) Wang, B.; Anthony, S. M.; Bae, S. C.; Granick, S. Anomalous yet Brownian. *Proc. Natl. Acad. Sci. U.S.A.* **2009**, *106*, 15160−15164.
(42) Chakrabarty, A.; Wang, F.; Sun, K.; Wei, Q.-H. Effects of translation-rotation coupling on the displacement probability distribution functions of boomerang colloidal particles. *Soft Matter* **2016**, *12*, 4318−4323.
(43) Koens, L.; Lisicki, M.; Lauga, E. The non-Gaussian tops and tails of diffusing boomerangs. *Soft Matter* **2017**, *13*, 2977−2982.
(44) Guan, J.; Wang, B.; Granick, S. Even hard-sphere colloidal suspensions display Fickian yet non-Gaussian diffusion. *ACS Nano* **2014**, *8*, 3331−3336.
(45) Jee, A.-Y.; Curtis-Fisk, J. L.; Granick, S. Nanoparticle diffusion in methycellulose thermoreversible association polymer. *Macromolecules* **2014**, *47*, 5793−5797.
(46) He, W.; Song, H.; Su, Y.; Geng, L.; Ackerson, B. J.; Peng, H. B.; Tong, P. Dynamic heterogeneity and non-Gaussian statistics for acetylcholine receptors on live cell membrane. *Nat. Commun.* **2016**, *7*, No. 11701.
(47) Lampo, T. J.; Stylianidou, S.; Backlund, M. P.; Wiggins, P. A.; Spakowitz, A. J. Cytoplasmic RNA-protein particles exhibit non-Gaussian subdiffusive behavior. *Biophys. J.* **2017**, *112*, 532−542.
(48) Slim, A. H.; Poling-Skutvik, R.; Conrad, J. C. Local confinement controls diffusive nanoparticle dynamics in semidilute polyelectrolyte solutions. *Langmuir* **2020**, *36*, 9153−9159.
(49) Wang, B.; Kuo, J.; Bae, S. C.; Granick, S. When Brownian diffusion is not Gaussian. *Nat. Mater.* **2012**, *11*, 481−485.
(50) Wong, I. Y.; Gardel, M. L.; Reichman, D. R.; Weeks, E. R.; Valentine, M. T.; Bausch, A. R.; Weitz, D. A. Anomalous diffusion probes microstructure dynamics of entangled F-actin networks. *Phys. Rev. Lett.* **2004**, *92*, No. 178101.
(51) Guo, H.; Bourret, G.; Lennox, R. B.; Sutton, M.; Harden, J. L.; Leheny, R. L. Entanglement-controlled subdiffusion of nanoparticles within concentrated polymer solutions. *Phys. Rev. Lett.* **2012**, *109*, No. 055901.
(52) Xue, C.; Zheng, X.; Chen, K.; Tian, Y.; Hu, G. Probing non-Gaussianity in confined diffusion of nanoparticles. *J. Phys. Chem. Lett.* **2016**, *7*, 514−519.
(53) Kohli, I.; Mukhopadhyay, A. Diffusion of nanoparticles in semidilute polymer solutions: Effect of different length scales. *Macromolecules* **2012**, *45*, 6143−6149.
(54) Poling-Skutvik, R.; Krishnamoorti, R.; Conrad, J. C. Size-dependent dynamics of nanoparticles in unentangled polyelectrolyte solutions. *ACS Macro Lett.* **2015**, *4*, 1169−1173.
(55) Doi, M.; Edwards, S. F. *The Theory of Polymer Dynamics*; Oxford University Press: New York, 1988; p 391.
(56) Fakhri, N.; MacKintosh, F. C.; Lounis, B.; Cognet, L.; Pasquali, M. Brownian motion of stiff filaments in crowded envionment. *Science* **2010**, *330*, 1804−1807.
(57) Nam, G.; Johner, A.; Lee, N.-K. Reptation of a semiflexible polymer through porous media. *J. Chem. Phys.* **2010**, *133*, 044908.
(58) Hölzer, A.; Sommerfeld, M. New simple correlation formula for the drag coefficient of non-spherical particles. *Powder Technol.* **2008**, *184*, 361−365.
(59) Loth, E. Drag of non-spherical solid particles of regular and irregular shape. *Powder Technol.* **2008**, *182*, 342−353.
(60) Mandø, M.; Rosendahl, L. On the motion of non-spherical particles at high Reynolds number. *Powder Technol.* **2010**, *202*, 1−13.
(61) Voth, G. A.; Soldati, A. Anisotropic particles in turbulence. *Annu. Rev. Fluid Mech.* **2017**, *49*, 249−276.
(62) Iannolo, G.; Minenkova, O.; Petruzzelli, R.; Cesareni, G. Modifying filamentous phage capsid: Limits in the size of the major capsid protein. *J. Mol. Biol.* **1995**, *248*, 835−844.
(63) Wang, Y. A.; Yu, X.; Overman, S.; Tsuboi, M.; Thomas, G. J.; Egelman, E. H. The structure of a filamentous bacteriophage. *J. Mol. Biol.* **2006**, *361*, 209−215.
(64) Sattar, S.; Bennett, N. J.; Wen, W. X.; Guthrie, J. M.; Blackwell, L. F.; Conway, J. F.; Rakonjac, J. Ff-nano, short functionalized nanorods derived from Ff (f1, fd or M13) filamentous bacteriophage. *Front. Microbiol.* **2015**, *6*, 316.
(65) Smith, D. E.; Perkins, T. T.; Chu, S. Dynamical scaling of DNA diffusion coefficients. *Macromolecules* **1996**, *29*, 1372−1373.
(66) Petrov, E. P.; Ohrt, T.; Winkler, R. G.; Schwille, P. Diffusion and segmental dynamics of double-stranded DNA. *Phys. Rev. Lett.* **2006**, *97*, 258101.

https://doi.org/10.1021/acs.macromol.1c00435
Macromolecules 2021, 54, 4557−4563